THE JOURNAL OF PHYSICAL CHEMISTRY Letters

Cite This: J. Phys. Chem. Lett. 2018, 9, 5598−5603

Letter

pubs.acs.org/JPCL

Superlattice Induced by Charge Order in the Organic Spin Chain $(TMTTF)_2X$ (X = SbF_6, AsF_6, and PF_6) Revealed by High-Field Electron Paramagnetic Resonance

Charles-Emmanuel Dutoit,[†] Anatoli Stepanov,[†] Johan van Tol,[‡] Maylis Orio,[§] and Sylvain Bertaina*[,†]

[†]Aix-Marseille Université, CNRS, IM2NP (UMR 7334), Marseille, France

[‡]National High Magnetic Field Laboratory, Florida State University, Tallahassee, Florida 32310, United States

[§]Aix-Marseille Université, CNRS, Central Marseille, ISM2, Marseille, France

ABSTRACT: We have investigated the charge ordering phase of the quasi-one-dimensional quantum antiferromagnet $(TMTTF)_2X$ (X = SbF_6, AsF_6, and PF_6) using high-fields/frequency electron paramagnetic resonance. In addition to the uniform displacement of the counteranions involved in the charge-order phase, we report the existence of a superlattice between the spin chains in the direction *c*, caused by the space modulation of the charge order. When the field is high enough, the magnetic decoupling of the spin chains allows us to estimate the interaction between the chains, J_c < 1 mK, three orders of magnitude lower than expected from the mean field theory.

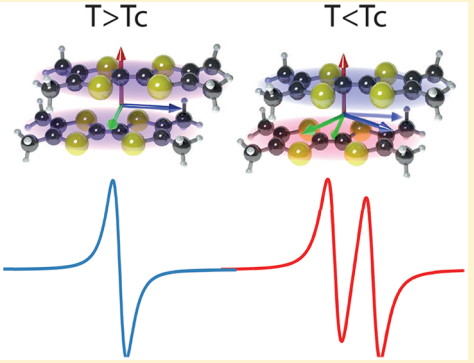

The family of quasi-1D organic conductors $(TMTTF)_2X$ is known to have a rich phase diagram with a sequence of competing ground states between spin-Peierls (SP), antiferromagnetic (AF), or superconductor states depending on the nature of counteranion X or external pressure. More particularly, the centro-symmetric X (X = SbF_6, AsF_6, and PF_6) is metallic at high temperatures, then it is an insulator, and finally, the ground state is either AF for SbF_6 (T_N = 8 K) or SP for AsF_6 (T_{SP} = 19K) and PF_6 (T_{SP} = 13 K). The metal−insulator transition was first observed by conductivity[1] and microwave measurements[2] and was attributed to a charge ordering (CO)[3,4] inside the molecule. At $T > T_{CO}$, the charge (hole) is equality divided between the two TMTTF molecules, then at $T < T_{CO}$ a displacement of charge from one TMTTF to the other induces a $4k_f$ ordering in the direction of the intrastack *a* axis (spin chain axis). The CO transition was considered structureless because no observation of the superlattice reflection was reported.[1] Since then, it has been proven that the X-ray was responsible for the destruction of the CO transition.[5,6] Only neutron scattering was able to directly show the displacement of the lattice during the CO transition.[7]

Figure 1 shows the elementary cell structure of $(TMTTF)_2X$. The electronic properties of this family of compounds are due to a hole shared by the two molecules of TMTTF. At high temperature ($T > T_{CO}$), the crystal structure is triclinic with a center of symmetry $P\bar{1}$. The distances between the sulfur atoms and the nearest counteranion are equal, $D_1 = D_2$, and the density of hole is the same on each TMTTF.[8] Below T_{CO}, the center of symmetry is removed, and the distances D_1 and D_2 are different, leading to a charge disproportion between the two molecules of TMTTF and, as a consequence, to the charge ordering.

The observation of the CO transition in $(TMTTF)_2X$ has been reported using many techniques. ^{13}C NMR investigations showed a splitting of lines below T_{CO}, caused by charge rearrangement around ^{13}C.[9,10] A minimum of the dielectric permittivity at T_{CO} = 156 K for X = SbF_6, T_{CO} = 103 K for X = AsF_6, and T_{CO} = 67 K for X = PF_6 has been reported by Monceau et al.,[11] and the role of the lattice in the CO has been studied by optic[12] and dilatometry[13,14] measurements.

Electron paramagnetic resonance (EPR) studies were also conducted. From the magnetic point of view, the hole carries an electronic spin *S* = 1/2. Because of the low symmetry of the structure, the principal axes of the *g* tensor and the crystallographic axes are different. Let us name the crystal axes *a*, *b*, and *c* and the magnetic axes a_m, b_m, and c_m. a_m, b_m, and c_m correspond to the minimum, intermediate, and maximum *g* factor, respectively. EPR is a tool of choice to measure with a high accuracy the *g* tensor in such organic crystals where the anisotropy of *g* factor is very weak.[15] In the high-temperature phase, the magnetic axes c_m and b_m are, respectively, parallel and perpendicular to the axis of the TMTTF molecule (Figure 1c) and are clearly different from the crystallographic axes. The a_m axis is perpendicular to the plane formed by the TMTTF and is close to the *a* axis, making with it an angle of ∼3°. Despite a weak magnetoelectric

Received: July 3, 2018
Accepted: August 7, 2018
Published: August 7, 2018

DOI: 10.1021/acs.jpclett.8b02070
J. Phys. Chem. Lett. 2018, 9, 5598−5603

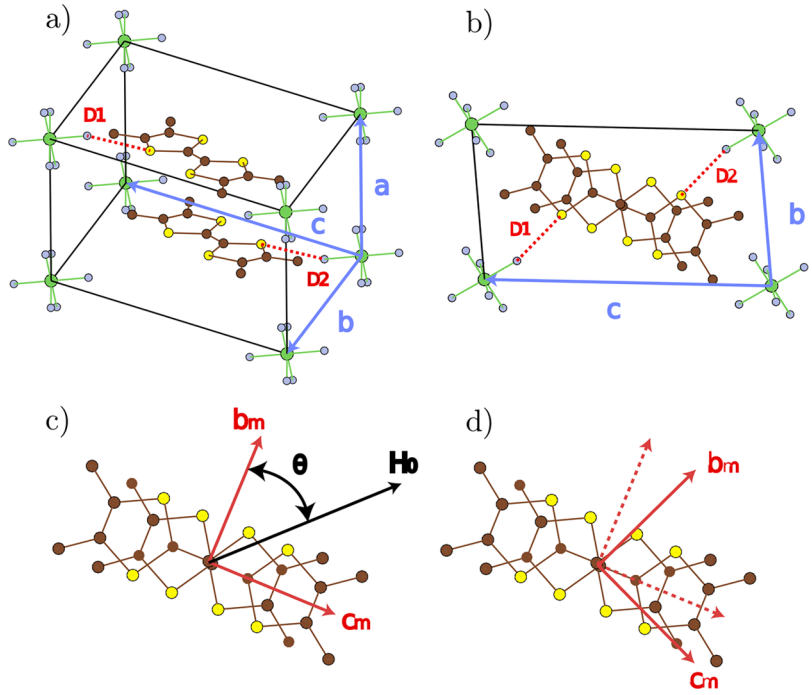

Figure 1. Crystallographic structure of $(TMTTF)_2X$. Two molecules of TMTTF (in the center of the cell) share one hole given by one of the eight counteranions X^- (X = SbF_6, AsF_6, or PF_6).

coupling, the EPR was able to detect the CO transition. Conductive EPR has shown a change of line asymmetry at T_{CO}.[16] A new source of line broadening below T_{CO} was reported.[17−19] On the basis of molecular density functional theory (DFT) calculations, the rotation of the principal axes of the g tensor was attributed to the CO transition.[20] This last result is represented in Figure 1c,d.

It is important to notice that all of these results have assumed or shown a uniform displacement of the anions.

The $(TMTTF)_2X$ family is also considered as a good prototype of quantum quasi-1D antiferromagnetic Heisenberg system (QQ1DAFH) with $J \approx 400$ K,[15,21,22] but the magnetic dimensionality remains controversial. Band structure calculations have shown a transfer integral inside the chain of $t_a \approx 200$ meV and between the chains $t_b \approx 40$ meV[23,24] and $t_c \approx 1$ meV[25] in the directions b and c, respectively. From a simple tight-binding model,[26] it follows that $J_a > J_b \gg J_c$. (Using $J_a \approx 400$ K, we estimate $J_b \approx 16$ K and $J_c \approx 0.01$ K.) But recently,[27] it has been shown that such values of the transfer integrals could lead to a more 2D magnetic behavior, and the application of QQ1DAFH models[28] might be wrong. Moreover, on account of the quasi-absence of electronic correlation in the c direction, the majority of theoretical and experimental studies probe the properties in the ab plane only.

In this Letter, we report a direct observation of superlattice in direction c, induced by the CO transition. Using high-field EPR, we demonstrate that in addition to the superlattice inside the chain axis the suppression of the center of symmetry also creates a superlattice between the chains, which is resolved when the magnetic field is large enough to decouple the chains in direction c. The decoupling of the chains allows us to estimate the coupling constant J_c.

Experimental Details. High-field/high-frequency EPR (HF-EPR) experiments have been carried out using a homemade quasioptical superheterodyn setup developed at NHMFL.[29] The spectrometer operates at 120, 240, and 336 GHz and at temperature from RT down to 2 K. The inhomogeneity of the field (crucial in our results) is <0.1 G across the volume of the samples. The presence of modulation coils allows us to record the first derivative of both the absorption and dispersion signals. The single crystals of $(TMTTF)_2X$ with X = SbF_6, AsF_6, and PF_6 have the shape of a needle with a typical size of $50 \times 100 \times 700$ μm^3, small enough to avoid polariton reflections inside the sample. The angular dependence of the EPR was measured by using a goniometer that rotates the sample in the plane perpendicular to the a axis. Because of the triclinic symmetry, the magnetic and crystallographic axes are different. The magnetic axes b_m and c_m correspond to the minimum and maximum of the resonance field, respectively. The temperature dependence of the EPR has been measured by applying the field at 45° between b_m and c_m. The HF-EPR spectra were recorded for the three systems and for the three available frequencies.

Charge-Order Transition Observed by HF-EPR. Figure 2 illustrates the detection of the CO transition by HF-EPR. At high temperature, the EPR line is a Lorentzian with a line width of ∼3 G close to the one reported at low frequency.[19] When $T < T_{CO}$, the line splits into two lines of nearly the same intensity. Examples of raw spectra are given in Figure 2a,b for X = AsF_6 and PF_6, respectively. For AsF_6, the splitting was observed at all available frequencies, whereas for SbF_6, it was observed at 240 and 336 GHz, and for PF_6, it was observed at 336 GHz only. The resonance fields of the compounds are reported in Figure 2c−e. The splitting is reversible (returning back to high temperature makes the lines to collapse) and reproducible (many samples from different batches have been used). It is clear that CO is responsible for the splitting of the EPR lines, but the physical interpretation is not trivial. It is known that CO removes the center of symmetry[30] and reduces the group from $P\bar{1}$ to P1. The electronic density is no longer equivalent between the two TMTTF molecules, which leads to two ^{13}C NMR signals.[9] However, the effect is different in the

DOI: 10.1021/acs.jpclett.8b02070
J. Phys. Chem. Lett. 2018, 9, 5598−5603

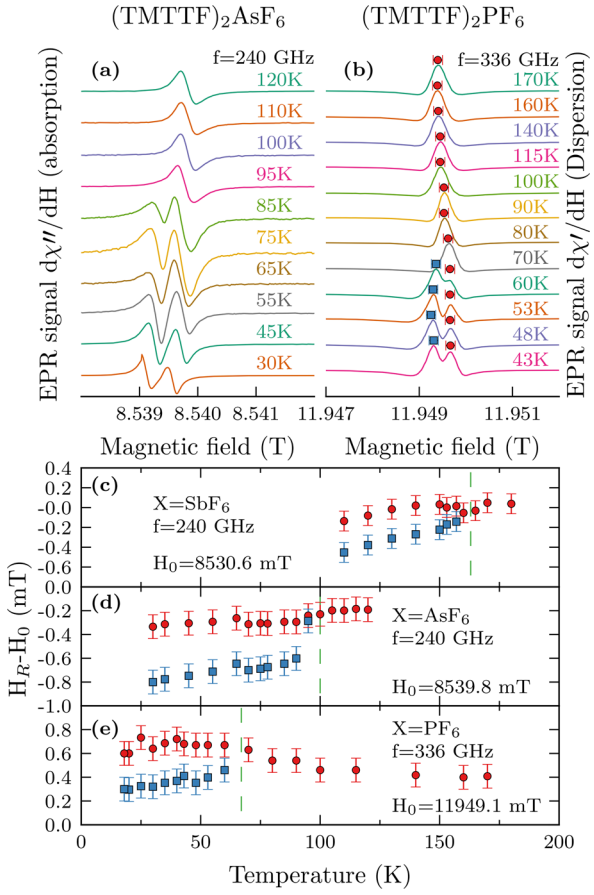

Figure 2. HF-EPR recorded at temperature above and below T_{CO} for the magnetic field at 45° between the magnetic axis b_m and c_m. (a) Derivative absorption signals of $(TMTTF)_2AsF_6$ at f = 240 GHz when the temperature decreases. (b) Derivative dispersion signals of $(TMTTF)_2PF_6$ at f = 336 GHz when the temperature decreases. The red circle and blue square are the resonance fields H_R and are reported as a function of temperature for (c−e) X = SbF_6, AsF_6 and PF_6 respectively. The vertical dashed lines represent T_{CO}. For clarity, the variation of H_R from the resonance field at high temperature H_0 is presented.

case of EPR, where only one electron spin is shared by the two TMTTF molecules, and thus only one signal is expected. Now, following the results of Riera and Poilblanc,[4] let us assume that the displacement of the anions is not fully uniform and has a small modulation in space. In Figure 3, we present two simple models. A and B are two representations of the unit cell in the CO state. In B, the displacement of the anions X is a bit stronger than in A. Consequently, in B, the electron-rich TMTTF molecule is a bit richer than in A. Although the charge disproportion has no direct effect on the spin, the counteranion displacement has a similar effect on the g tensor. In triclinic symmetry, the orientation of g-tensor axes is not fixed by the symmetry, and the displacement of X induces a rotation of the tensor principal axes.[20] A similar effect has been reported for other low-symmetry systems.[31,32] In configuration B, the displacement is stronger than in A, which leads to a more significant rotation of the g tensor of the configuration B than in A.

Exchange Splitting. The ability to resolve the two EPR lines coming from the A and B configurations depends on the relative value of the mismatch of the Zeeman energies for the two nonequivalent spins, $\Delta g\mu_B H$, and on the Heisenberg

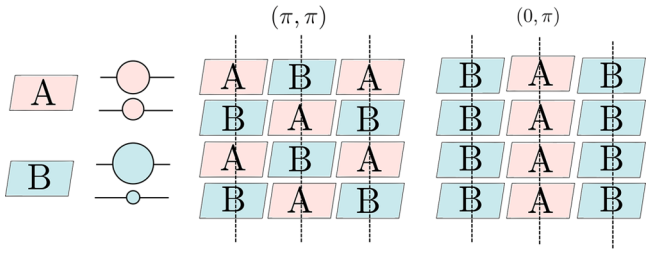

Figure 3. Schematic representation of CO superlattice inspired from the original work of Riera and Poilblanc.[4] A and B are unit cells of $(TMTTF)_2X$ in the CO configuration (i.e., with charge density displacement), but B has a stronger charge displacement than A. The vertical dashed lines represent the chain axis. The (π,π) configuration alternates A and B in both directions, whereas $(0,\pi)$ has a uniform A or B inside the chain but alternates between the chains.

exchange interaction in the direction i, k_BJ_i. When the magnetic field is smaller than the exchange interaction, the signals from the two non equivalent sites are merged into one line due to fast fluctuation, as predicted by the theory of exchange narrowing.[33,34] On the contrary, the lines from the two nonequivalent magnetic sites are split[35] in the case of strong magnetic field

$$\Delta g\mu_B H > k_B J_i \quad (1)$$

Here Δg is the difference of the g factors of the two nonequivalent sites; it is a maximum at 45° between b_m and c_m. This condition, mathematically proven by Anderson,[36] was used to directly estimate the interchain coupling in the quantum spin chain $CuGeO_3$.[37] The intrachain exchange interaction of $(TMTTF)_2X$ (~400 K) is too large, and all of the chains in the configuration (π,π) in Figure 3 should have the same resonance field (only one line is expected). In the configuration $(0,\pi)$, two kinds of chains exist: full A and full B. Compared with ref 4, the configuration (π,π) is scenario c, $(\pi,0)$ is scenario d, (0,0) is scenario a (and is the standard picture to explain the CO transition), and $(0,\pi)$ is not mentioned. Because we can resolve two lines, we are able to decouple the signals from two different chains. Thus we are able to give an upper limit for the smallest interchain coupling J_c.

To our knowledge, this is the first experimental estimation of the interaction between chains of $(TMTTF)_2X$ in direction c, and this result has remarkable implications for the magnetic properties.

It confirms the quasi-absence of electronic correlation in the c direction. Band structure calculations have managed to estimate the transfer integral in the a (chain axis) and b directions,[23,24] but only one paper, so far, has reported a theoretical prediction in the c direction, $t_c \approx 1$ meV, which leads in the tight-binding model to $J_c = (t_c/t_a)^2 J \approx 10$ mK,[25] one order of magnitude higher than what we get but not so far away from theoretical predictions using mean field models. Indeed, the magnetic dimensionality has to be carefully considered. Although the $(TMTTF)_2X$ family is a QQ1DAFH system, the large difference between J_b and J_c makes some models fail. One remarkable example is the estimation of the interchain coupling J' from the Néel order temperature[28,38]

$$J' = 1.073 T_N^{1D} / \sqrt{\ln\left(\frac{2.6J}{T_N^{1D}}\right) + \frac{1}{2}\ln\ln\left(\frac{2.6J}{T_N^{1D}}\right)} \quad (2)$$

DOI: 10.1021/acs.jpclett.8b02070
J. Phys. Chem. Lett. 2018, 9, 5598−5603

which gives for $(TMTTF)_2SbF_6$, $J' \approx 2$ K, three orders of magnitude higher than the value we found. The reason comes from the assumptions made to develop the standard model by Irkin and Katanin[38] then Yasuda et al.:[28] The chain is coupled to the nearest neighbor chains by the same interaction. This is not the case for $(TMTTF)_2SbF_6$. More surprisingly, Yoshimi et al.[27] have shown that in the CO state the intersite Coulomb repulsion could lead to an exchange interaction of the same order in direction a and b. However, this last result is not confirmed by our experimental results, since a QQ2DAFH should have a much higher Néel temperature, even with the weak J_c we report. Using the equation connecting the Néel temperature and the interlayer coupling J'[28]

$$T_N^{2D} = 0.732\pi J/\left(2.43 - \ln\left(\frac{J'}{J}\right) - \ln\left(\frac{T_N^{2D}}{J}\right)\right) \quad (3)$$

with $J = 400$ K and $J' = 1$ mK, we find $T_N^{2D} = 54$ K, while $T_N^{1D} = 3$ mK from eq 2. In both cases, the model fails to describe $(TMTTF)_2SbF_6$. Our results should help the extension of the 1D and 2D models connecting T_N and the exchange couplings[28,38] to the cases of intermediate dimensionality, $J_a > J_b \gg J_c$.

Charge Ordering and the Superlattice in the c Direction. To understand the role of the CO transition on the appearance of a magnetic superlattice in direction c, we performed EPR measurements for several orientations in the plane perpendicular to the chain axis. Figure 4 shows the variation of the resonance field as a function of the angle θ in $(TMTTF)_2AsF_6$ for $f = 336$ GHz above (black diamonds) and below (red circles and blue squares) T_{CO}. $\theta = 0°$ corresponds to the maximum of the resonance field at $T = 110$ K. At $T < T_{CO}$ the splitting of the EPR line is accompanied by a rotation of the g tensor. The rotation is not the same for the two lines. In the case of line 1, we found a rotation through 3°, whereas for line 2 the angle of rotation is 11°. The rotation of the principal axes of the g-tensor was observed at low field in nonresolved EPR spectra and explained by the displacement of the anions X.[20] The modulation of the stain field in c direction induces two kinds of anion displacements leading to 2 different rotations of the g-tensor which can be resolved at high field.

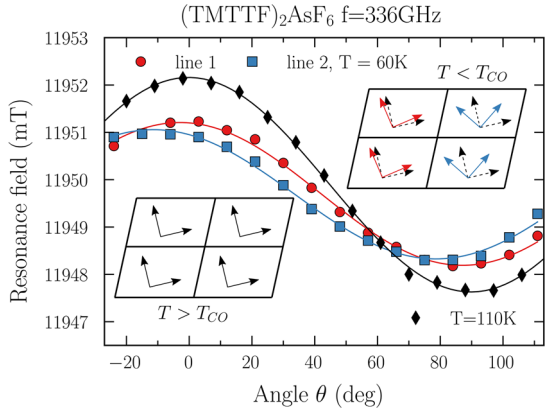

Figure 4. Resonance field of $(TMTTF)_2AsF_6$ recorded in the plane perpendicular to the chain axis. The black diamonds represent the line at $T = 110$ K (above T_{CO}), while the red circles and the blue squares are the two lines observed at $T = 60$ K (below T_{CO}). The lines are the best fits. The insets represent the g-tensor axes in the plane perpendicular to the chain axis. At $T > T_{CO}$, all of the chains are equivalent. At $T < T_{CO}$, two inequivalent chains have different orientations of their g tensors.

The relative rotation of the g tensor ($\Delta\theta$) of two adjacent chains was also assumed to explain the EPR line broadening for $T < T_{CO}$ at lower frequencies.[39] However, neither the rotation axis nor the amplitude of the rotation is coherent with our results. The reason is that the authors used the anisotropic Zeeman effect (AZE)[40] to extract quantitative information from the EPR line width. Unfortunately, this model needs the interchain coupling J', and in the absence of a reliable value, the authors estimated J' using ref 28, which, as we have shown previously, is irrelevant in the case of $(TMTTF)_2X$ salts. Using $J' = 1.1$ K and an enhanced line width of 1.5 G, they found a large relative rotation of $\Delta\theta = \pm 32°$ about the b axis. Now let us approach the problem from the other side by using our direct measurement of $\Delta\theta = \pm 4°$ about the a axis, which yields $\Delta g \approx 2 \times 10^{-4}$, and the experimental results obtained in the W band from ref 39 ($\Delta H = 1.5$ G and $H_0 = 3.36$ T). Applying the AZE model

$$J' = \sqrt{\pi/8}\, H_0^2 |\Delta g|^2/(g_e \Delta H) \quad (4)$$

we find $J' \approx 0.9$ mK, which is coherent with our values of J_c (Table 1).

Table 1. Estimation of the Interchain Coupling J_c[a]

X =	Δg	minimum frequency/(field) to resolve the splitting	upper limit J_c
AsF_6	12×10^{-5}	120 GHz (4.28 T)	5 G (~0.7 mK)
SbF_6	9×10^{-5}	240 GHz (8.56 T)	8 G (~1 mK)
PF_6	7×10^{-5}	336 GHz (12 T)	8 G (~1 mK)

[a] Δg is the difference of the g factors of the two nonequivalent sites for $\theta = 45°$. The frequencies/fields correspond to the threshold where the splitting has been resolved. Using eq 1, we estimate the upper limit of the interchain coupling.

Figure 5 demonstrates how EPR can probe the CO transition. In Figure 5a, the TMTTF (brown) molecules are stacked in the a direction and form the chain axis. They are separated by the counteranions X (PF_6, AsF_6, SbF_6) (green). Because of the low triclinic symmetry of the system, the crystallographic axes and the magnetic axes are different. For $T > T_{CO}$, the two TMTTF molecules are equivalent and the magnetic axes c_m and b_m coincide with the symmetry axes of the TMTTF. At the CO phase transition (Figure 5b), the symmetry is reduced by removing the centers of inversion, the counteranion X cages are shifted, and the charge balance on the two TMTTF is broken. One TMTTF (blue) has a higher charge density than the second one (red). Because the g tensor is sensitive to the electronic change,[20] it turns about the a axis (as shown by low-field EPR[20,41]). The vertical sinusoidal curve represents the change of the electronic density. Figure 5c shows how the high-field/high-frequency EPR revealed that the CO is not uniform and a CO in the c direction is also induced. In the chains with light (dark) red and blue TMTTF, the charge displacement is less (more) pronounced. As a consequence, the rotation of the g tensor is less (more) significant, resulting in line 1 (line 2).

Finally, let us discuss why the superlattice in the c direction was not detected by other techniques. In the introduction to this paper we have presented several techniques that have permitted the observation of the CO. However, only a few of them, such as ^{13}C NMR or neutron scattering, have the

DOI: 10.1021/acs.jpclett.8b02070
J. Phys. Chem. Lett. 2018, 9, 5598−5603

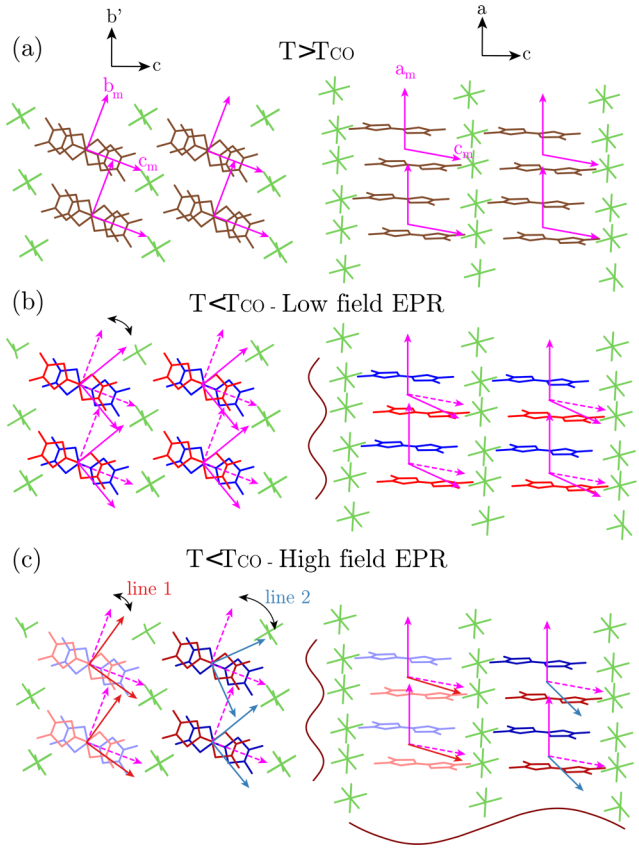

Figure 5. Schematic representation of the structural and magnetic properties of $(TMTTF)_2X$. The left column represents four unit cells in the plane perpendicular to the chain axis *a*, whereas the right side is four unit cells in the plane *ac*. (a) At $T > T_{CO}$, the charge density is equally distributed between the TMTTF molecules (brown). The principal axis of the *g* tensor (pink) is oriented along the TMTTF molecular axes. All unit cells are magnetically equivalent. (b) At $T < T_{CO}$, the charge density of the two TMTTF molecules is no longer balanced, and the *g*-tensor axes rotate about the *a* axis.[20] (c) High-field/high-frequency EPR experiments reveal that this rotation is not uniform due to modulation of the charge ordering. The charge unbalance is stronger in one stack (dark blue and red) than in the second (light blue and red), leading to two different rotations of the *g*-tensor axes and thus to two EPR lines.

spectral or spatial resolution to detect the interchain CO modulation. In the case of ^{13}C NMR, the main CO was detected by observing the splitting of ^{13}C NMR lines, but, as seen in figures 2 and 4 of ref 9, this splitting is very small. It is not surprising that a modulation of the CO would lead to a second separation of each line that is too tiny to be resolved. The measurement of the displacement of the counteranions responsible for the CO was a challenging neutron scattering experiment.[7] The modulation of the displacement would just be included in the error bars. In our case the observation of the CO modulation was possible because: (i) The low P_1 symmetry allows the rotation of the *g*-tensor axes. In higher symmetry, this effect would not exist. (ii) The very small line width of the organic salts ($\Delta H \approx 1$ G) allows us to resolve the two EPR lines. (iii) The two EPR lines are not collapsed by the interchain exchange interaction because electronic correlations in the *c* direction were nearly absent and the magnetic field was high (exchange splitting regime[36]).

In conclusion, the CO transition observed in $(TMTTF)_2X$ ($X = SbF_6$, AsF_6, PF_6) is accompanied by a displacement of the counteranions X. This displacement was observed by neutron,[7] NMR,[9] and dilatometry[11] but was considered uniform[13] all over the crystal. Using high-field/frequency EPR, we have seen the signal of two nonequivalent spin chains. We have interpreted this result as a modulation of the displacement of X in the direction *c*, leading to two orientations of the *g* tensor and consequently to two EPR lines.

The line splitting allows us to estimate the exchange coupling in the *c* direction ($J_c \approx 1$ mK). Using this value, we have shown that neither the 1D model (eq 2) nor the 2D one (eq 3) can describe $(TMTTF)_2SbF_6$. We believe that this result should stimulate the development of a theory linking T_N and the interchain couplings in the case $J_a > J_b \gg J_c$.

AUTHOR INFORMATION

Corresponding Author

*E-mail: sylvain.bertaina@im2np.fr.

ORCID

Maylis Orio: 0000-0002-9317-8005

Sylvain Bertaina: 0000-0002-6466-8830

Notes

The authors declare no competing financial interest.

ACKNOWLEDGMENTS

We acknowledge M. Dressel for providing the sample. We thank M. Kuzmin and S. Todo for stimulating discussions. This work was supported by NSF Grant No. DMR-1206267, CNRS-PICS CoDyLow, and CNRS's infrastructure of research RENARD (FR3443) for EPR facilities. The NHMFL is supported by the NSF Cooperative Agreement Grant No. DMR-1157490 and the State of Florida.

REFERENCES

(1) Laversanne, R.; Coulon, C.; Gallois, B.; Pouget, J.; Moret, R. Structural and electrical properties of $(TMTTF)_2MF_6$ salts (M = P, As, Sb). Role of the anions. *J. Phys., Lett.* **1984**, *45*, 393−399.

(2) Javadi, H. H. S.; Laversanne, R.; Epstein, A. J. Microwave conductivity and dielectric constant of tetramethyltetrathiafulvalene salts [$(TMTTF)_2X$, X = SCN, ReO_4, SbF_6. *Phys. Rev. B: Condens. Matter Mater. Phys.* **1988**, *37*, 4280−4283.

(3) Shibata, Y.; Nishimoto, S.; Ohta, Y. Charge ordering in the one-dimensional extended Hubbard model: Implication to the TMTTF family of organic conductors. *Phys. Rev. B: Condens. Matter Mater. Phys.* **2001**, *64*, 235107.

(4) Riera, J.; Poilblanc, D. Influence of the anion potential on the charge ordering in quasi-one-dimensional charge-transfer salts. *Phys. Rev. B: Condens. Matter Mater. Phys.* **2001**, *63*, 241102.

(5) Foury-Leylekian, P.; Le Bolloc'h, D.; Hennion, B.; Ravy, S.; Moradpour, A.; Pouget, J.-P. Neutron-scattering evidence for a spin-Peierls ground state in $(TMTTF)_2PF_6$. *Phys. Rev. B: Condens. Matter Mater. Phys.* **2004**, *70*, 4−7.

(6) Coulon, C.; Foury-Leylekian, P.; Fabre, J.-M.; Pouget, J.-P. Electronic instabilities and irradiation effects in the $(TMTTF)_2X$ series. *Eur. Phys. J. B* **2015**, *88*, 85.

(7) Foury-Leylekian, P.; Petit, S.; Andre, G.; Moradpour, A.; Pouget, J. Neutron scattering evidence for a lattice displacement at the charge ordering transition of. *Phys. B* **2010**, *405*, S95−S97.

(8) Pouget, J. P.; Ravy, S. Structural Aspects of the Bechgaard Salts and Related Compounds. *J. Phys. I* **1996**, *6*, 1501−1525.

(9) Chow, D. S.; Zamborszky, F.; Alavi, B.; Tantillo, D. J.; Baur, A.; Merlic, C. A.; Brown, S. E. Charge Ordering in the TMTTF Family of Molecular Conductors. *Phys. Rev. Lett.* **2000**, *85*, 1698−1701.

(10) Zamborszky, F.; Yu, W.; Raas, W.; Brown, S.; Alavi, B.; Merlic, C.; Baur, A. Competition and coexistence of bond and charge orders

DOI: 10.1021/acs.jpclett.8b02070
J. Phys. Chem. Lett. 2018, 9, 5598−5603

in $(TMTTF)_2AsF_6$. *Phys. Rev. B: Condens. Matter Mater. Phys.* **2002**, *66*, 081103.
(11) Monceau, P.; Nad, F. Y.; Brazovskii, S. Ferroelectric mott-hubbard phase of organic $(TMTTF)_2X$ conductors. *Phys. Rev. Lett.* **2001**, *86*, 4080−4083.
(12) Dumm, M.; Abaker, M.; Dressel, M.; Montgomery, L. K. Charge order in $(TMTTF)_2PF_6$ investigated by infrared spectroscopy. *J. Low Temp. Phys.* **2006**, *142*, 609−612.
(13) De Souza, M.; Foury-Leylekian, P.; Moradpour, A.; Pouget, J.-P.; Lang, M. Evidence for Lattice Effects at the Charge-Ordering Transition in $(TMTTF)_2X$. *Phys. Rev. Lett.* **2008**, *101*, 216403.
(14) De Souza, M.; Hofmann, D.; Foury-Leylekian, P.; Moradpour, A.; Pouget, J. P.; Lang, M. Exploring the charge-ordering transition in $(TMTTF)_2X$ via thermal expansion measurements. *Phys. B* **2010**, *405*, S92−S94.
(15) Coulon, C.; Clérac, R. Electron spin resonance: a major probe for molecular conductors. *Chem. Rev.* **2004**, *104*, 5655−88.
(16) Coulon, C.; Lalet, G.; Pouget, J.; Foury-Leylekian, P.; Moradpour, A.; Fabre, J. Anisotropic conductivity and charge ordering in $(TMTTF)_2X$ salts probed by ESR. *Phys. Rev. B: Condens. Matter Mater. Phys.* **2007**, *76*, 1−13.
(17) Furukawa, K.; Hara, T.; Nakamura, T. Deuteration Effect and Possible Origin of the Charge-Ordering Transition of $(TMTTF)_2X$. *J. Phys. Soc. Jpn.* **2005**, *74*, 3288−3294.
(18) Nakamura, T. ESR Investigation of Charge Localized States in $(TMTTF)_2X$. *Synth. Met.* **2003**, *137*, 1181−1182.
(19) Nakamura, T. Possible Charge Ordering Patterns of the Paramagnetic Insulating States in $(TMTTF)_2X$. *J. Phys. Soc. Jpn.* **2003**, *72*, 213−216.
(20) Dutoit, C.-E.; Bertaina, S.; Orio, M.; Dressel, M.; Stepanov, A. Charge-ordering induces magnetic axes rotation in organic materials $(TMTTF)_2X$ (with X = SbF_6, AsF_6, and PF_6). *Low Temp. Phys.* **2015**, *41*, 942−944.
(21) Dumm, M.; Loidl, A.; Fravel, B.; Starkey, K.; Montgomery, L.; Dressel, M. Electron spin resonance studies on the organic linear-chain compounds $(TMTCF)_2X$ (C = S,Se; X = PF_6,AsF_6,ClO_4,Br). *Phys. Rev. B: Condens. Matter Mater. Phys.* **2000**, *61*, 511−521.
(22) Foury-Leylekian, P.; Petit, S.; Coulon, C.; Hennion, B.; Moradpour, A.; Pouget, J.-P. Inelastic neutron scattering investigation of magnetic excitations in the spin-Peierls ground state of. *Phys. B* **2009**, *404*, 537−540.
(23) Granier, T.; Gallois, B.; Ducasse, L.; Fritsch, A.; Filhol, A. 4 K crystallographic and electronic structures of $(TMTTF)_2X$ salts (X^-= PF_6^-, AsF_6^-. *Synth. Met.* **1988**, *24*, 343−356.
(24) Giovannetti, G.; Kumar, S.; Pouget, J.-P.; Capone, M. Unraveling the polar state in $TMTTF_2$-PF_6 organic crystals. *Phys. Rev. B: Condens. Matter Mater. Phys.* **2012**, *85*, 205146.
(25) Grant, P. The C-axis Interaction In $(TMTSF)_2X$. *Le Journal de Physique Colloques* **1983**, *44*, C3-1121−C3-1124.
(26) Seo, H.; Merino, J.; Yoshioka, H.; Ogata, M. Theoretical aspects of charge ordering in molecular conductors. *J. Phys. Soc. Jpn.* **2006**, *75*, 051009.
(27) Yoshimi, K.; Seo, H.; Ishibashi, S.; Brown, S. Tuning the Magnetic Dimensionality by Charge Ordering in the Molecular TMTTF Salts. *Phys. Rev. Lett.* **2012**, *108*, 096402.
(28) Yasuda, C.; Todo, S.; Hukushima, K.; Alet, F.; Keller, M.; Troyer, M.; Takayama, H. Néel Temperature of Quasi-Low-Dimensional Heisenberg Antiferromagnets. *Phys. Rev. Lett.* **2005**, *94*, 217201.
(29) van Tol, J.; Brunel, L.-C.; Wylde, R. J. A quasioptical transient electron spin resonance spectrometer operating at 120 and 240 GHz. *Rev. Sci. Instrum.* **2005**, *76*, 074101.
(30) Nad, F.; Monceau, P.; Carcel, C.; Fabre, J. M. Dielectric response of the charge-induced correlated state in the quasi-one-dimensional conductor $(TMTTF)_2PF_6$. *Phys. Rev. B: Condens. Matter Mater. Phys.* **2000**, *62*, 1753−1756.
(31) van Rens, J. G. M.; Keijzers, C. P.; van Willigen, H. Single-Crystal EPR Study of a Cu(II)dialkyldiselenocarbamate. An Example of Noncoinciding Principal Axes. *J. Chem. Phys.* **1970**, *52*, 2858−2864.
(32) Pilbrow, J. R.; Wood, C. S. Rotation of tensor axes in the EPR of Cr^{3+} in monoclinic sites. *J. Magn. Reson. (1969-1992)* **1979**, *34*, 113−122.
(33) Anderson, P.; Weiss, P. Exchange Narrowing in Paramagnetic Resonance. *Rev. Mod. Phys.* **1953**, *25*, 269−276.
(34) Kubo, R.; Tomita, K. A General Theory of Magnetic Resonance Absorption. *J. Phys. Soc. Jpn.* **1954**, *9*, 888−919.
(35) Hennessy, M. J.; McElwee, C. D.; Richards, P. M. Effect of Interchain Coupling on Electron-Spin Resonance in Nearly One-Dimensional Systems. *Phys. Rev. B* **1973**, *7*, 930−947.
(36) Anderson, P. W. A Mathematical Model for the Narrowing of Spectral Lines by Exchange or Motion. *J. Phys. Soc. Jpn.* **1954**, *9*, 316−339.
(37) Nojiri, H.; Ohta, H.; Miura, N.; Motokawa, M. Study of spin-Peierls $CuGeO_3$ by high-field ESR. *Phys. B* **1998**, *246−247*, 16−21.
(38) Irkhin, V.; Katanin, A. Calculation of Neel temperature for S = 1/2 Heisenberg quasi-one-dimensional antiferromagnets. *Phys. Rev. B: Condens. Matter Mater. Phys.* **2000**, *61*, 6757−6764.
(39) Yasin, S.; Salameh, B.; Rose, E.; Dumm, M.; Krug von Nidda, H.-a.; Loidl, A.; Ozerov, M.; Untereiner, G.; Montgomery, L.; Dressel, M. Broken magnetic symmetry due to charge-order ferroelectricity discovered in $(TMTTF)_2X$ salts by multifrequency ESR. *Phys. Rev. B: Condens. Matter Mater. Phys.* **2012**, *85*, 144428.
(40) Pilawa, B. Anisotropy of the electron spin-resonance linewidth of $CuGeO_3$. *J. Phys.: Condens. Matter* **1997**, *9*, 3779−3792.
(41) Furukawa, K.; Hara, T.; Nakamura, T. Anomalous Temperature Dependence of g -Tensor in Organic Conductor, $(TMTTF)_2$ X (X = Br, PF_6, and SbF_6). *J. Phys. Soc. Jpn.* **2009**, *78*, 104713.

DOI: 10.1021/acs.jpclett.8b02070
J. Phys. Chem. Lett. 2018, 9, 5598−5603